

Articles

# Surface Plasmon Resonance Imaging Measurements of the Inhibition of Shiga-like Toxin by Synthetic Multivalent Inhibitors

Vishal Kanda, Pavel Kitov, David R. Bundle, and Mark T. McDermott\*

Department of Chemistry, University of Alberta, Edmonton, AB, Canada T6G 2G2

A variety of new methodologies to pattern biomolecules on surfaces and to detect binding events are currently being developed for high-throughput assay applications. Carbohydrates serve as attachment sites for toxins, bacteria, and viruses. Immobilized carbohydrate units can thus be used to directly detect these agents or as a platform for inhibitor assessment. In this work, modified glycosides were patterned on gold surfaces to monitor the binding of the homopentameric B<sub>5</sub> cell-recognition subunit of the Shiga-like toxin (SLT). Binding was detected with the label-free method of surface plasmon resonance (SPR) imaging. Two synthetic multivalent inhibitors were used in order to effect inhibitory binding, and SPR imaging is presented as a simple alternative to ELISA for the study of toxin inhibition. In contrast to existing methods for the study of carbohydrate–protein interactions, in particular ELISA, the use of micropatterned sensor surfaces is shown to be advantageous due to a decrease in complications and manual labor from numerous blocking, washing, and labeling steps. Carbohydrate receptor density on the sensor surface was optimized in order to effect the maximum binding of the SLT. The IC<sub>50</sub> values determined were in the low-nanomolar range for each of the two inhibitors studied.

In recent years, much research effort has been directed at the development of microarray methods for the parallel analysis of interactions in proteomics and genomics. In addition to these widely known areas of research, there is a growing interest in the analysis of biological interactions mediated by carbohydrates, or “glycomics”.<sup>1,2</sup> The expansion of research efforts in this area

is being driven by the role carbohydrate ligands play in mediating various biological phenomena. Research has unraveled a large, diverse family of carbohydrate-mediated interactions between cells and viruses, bacteria, extracellular matrix scaffolds, and other cells.<sup>3</sup> Cell surfaces can interact with other cells through a variety of interactions involving membrane-bound and extracellular oligosaccharides, glycolipids, and glycoproteins.

Among the challenges in the study of carbohydrates is their relative structural complexity. The presence of multiple branching points, stereochemistry, and functional group modifications in natural systems introduces a higher degree of synthetic difficulty for oligosaccharides in comparison to oligonucleotides and linear polypeptides.<sup>4,5</sup> Much of the functional activity of carbohydrates is governed by highly specific recognition with proteins. Increasing interest in examining the functional characteristics of carbohydrate ligands as well as the need for throughput and efficiency in the analysis of carbohydrate interactions is leading to a surge in microarray research.<sup>2,6–10</sup> The sheer variety of structures and interactions make a high-throughput analysis system such as microarrays a necessity for expansion of research into glycomics.

Lectins are a class of proteins that function as receptors for specific carbohydrate moieties.<sup>4,11,12</sup> The interactions of individual

- (2) Wang, D.; Liu, S.; Trummer, B. J.; Deng, C.; Wang, A. *Nat. Biotechnol.* **2002**, *20*, 275–281.
- (3) Mammen, M.; Choi, S.-K.; Whitesides, G. M. *Angew. Chem., Int. Ed.* **1998**, *37*, 2754–2794.
- (4) Bertozzi, C.; Kiessling, L. L. *Science* **2001**, *291*, 2357–2364.
- (5) Houseman, B. T.; Mrksich, M. In *Host–Guest Chemistry*; Penades, S., Ed.; Springer-Verlag: Berlin, 2002; Vol. 218, pp 1–44.
- (6) Smith, E. A.; Thomas, W. D.; Kiessling, L. L.; Corn, R. M. *J. Am. Chem. Soc.* **2003**, *125*, 6140–6148.
- (7) Fang, Y.; Frutos, A. G.; Lahiri, J. *Langmuir* **2003**, *19*, 1500–1505.
- (8) Houseman, B. T.; Mrksich, M. *Chem. Biol.* **2002**, *9*, 443–454.
- (9) Park, S.; Lee, M.-R.; Pyo, S.-J.; Shin, I. *J. Am. Chem. Soc.* **2004**, *126*, 4812–4819.
- (10) Disney, M. D.; Seeberger, P. H. *Chem. Eur. J.* **2004**, *10*, 3308–3314.
- (11) Sharon, N.; Lis, H. *Science* **1989**, *246*, 227–246.

\* To whom correspondence should be addressed. E-mail: mark.mcdermott@ualberta.ca. Voice: 780-492-3687. Fax: 780-492-8231.

(1) Feizi, T. *Glycoconjugate J.* **2000**, *17*, 553–565.

carbohydrate moieties with proteins are weak, with typical dissociation constants in the high-micromolar to millimolar range.<sup>13,14</sup> As a consequence, many lectins interact with their targets via multiple, homologous binding sites in order to increase affinity. A well-studied example is that of the influenza virus, which binds to cell surface sialic acids via a homotrimeric lectin group. The initial binding allows other lectin groups on the viral surface to come into contact with more cell surface sugars, eventually deforming the cell membrane and leading to endocytosis.<sup>3</sup>

The *Escherichia coli* bacterium produces toxins implicated in a number of gastrointestinal maladies including diarrhea, hemorrhagic colitis, and the hemolytic uremic syndrome.<sup>15</sup> The verotoxins belong to a class of toxins also known as Shiga-like toxins (SLTs) due to their structural similarity to the Shiga toxin produced by *Shigella dysenteriae* type I. Shiga-like toxins consist of a 38.4-kDa pentameric B<sub>5</sub> subunit, which is responsible for the recognition of cell surface oligosaccharide units, and a 32-kDa enzyme portion, the A subunit, which damages ribosomal RNA once internalized by the cell.<sup>16</sup> The cell surface recognition is a necessary step in allowing the toxin to be internalized and fulfill its enzymatic function. In mammalian cells, the Gb<sub>3</sub> glycolipid is the recognition element responsible for the binding of the Shiga toxins.<sup>17</sup> The carbohydrate portion of the Gb<sub>3</sub> glycolipid is the P<sup>k</sup> trisaccharide ( $\alpha$ -D-Galp-(1-4)- $\beta$ -D-Galp-(1-4)- $\beta$ -D-Glcp). It has been shown that the binding sites of the B<sub>5</sub> subunit can be blocked with synthetic ligands containing multiple copies of the P<sup>k</sup> trisaccharide unit.<sup>16</sup> The 5-fold quasi-symmetric ligands can bind to all five of the strong binding sites on the B<sub>5</sub> subunit simultaneously, effectively inhibiting the toxin.<sup>16,18</sup> This system is used here to establish the utility of SPR imaging for studies of toxin binding inhibition.

SPR has previously been applied to the elucidation of binding constants for various carbohydrate-protein interactions,<sup>19</sup> especially those associated with pathogens.<sup>3,20</sup> Some noteworthy examples that have been studied by SPR include the binding of HIV-1 protein gp120 to potential inhibitors composed of glycodendrimers and sulfated dextran,<sup>21</sup> the binding of the toxin ricin to various synthetic glycolipids,<sup>22,23</sup> and the interactions of cholera toxin with ganglioside receptors.<sup>24,25</sup> The sensitivity and perceived

accuracy of the analytical data from SPR measurements, as well as the ease of use of commercial instrumentation, have allowed researchers to ascertain binding constants from analysis of kinetic data.

Relevant to the present work, SPR imaging has been used to study protein-carbohydrate interactions in array format.<sup>6</sup> Interactions between immobilized monosaccharides and proteins in noncompetitive and competitive format were analyzed. In this work, we fabricate arrays of di- and trisaccharides to study the binding of SLT. These arrays are employed to explore the inhibitory effect of two synthetic compounds capable of multivalent binding to SLT. We compare the methodology developed here to that previously used to examine SLT inhibition.

## EXPERIMENTAL SECTION

HS(CH<sub>2</sub>)<sub>11</sub>(OCH<sub>2</sub>CH<sub>2</sub>)<sub>3</sub>OCH<sub>3</sub> (EG3-OMe) was synthesized in accordance with known procedures.<sup>26,27</sup> The structures of the two probe glycosides used are shown in Figure 1. The syntheses of bis{16-[4-O-[4-O-( $\alpha$ -D-galactopyranosyl)- $\beta$ -D-galactopyranosyl]- $\beta$ -D-glucopyranosyloxy]hexadecanyl}disulfide (C<sub>16</sub>P<sup>k</sup>) and bis{16-[4-O-(2-acetamido-2-deoxy- $\beta$ -D-galactopyranosyl)- $\beta$ -D-glucopyranosyloxy]-hexadecanyl}disulfide (C<sub>16</sub>AGM<sub>2</sub>) were published previously.<sup>28</sup> The inhibitors studied are shown in Figure 2. The synthesis of the daisy inhibitor was reported previously,<sup>29</sup> and the synthesis of the starfish-2 inhibitor (SF-2) is presented in the supplementary information to this paper.

The recombinant SLT was expressed without the enzymatic A subunit, leaving only the self-assembling B<sub>5</sub> subunit containing the carbohydrate recognition sites and purified according to published procedures.<sup>30</sup> A 1.6 mg/mL concentration of SLT in PBS with 0.02% NaN<sub>3</sub> as preservative was used as a stock solution. Protein solutions were diluted in phosphate-buffered saline (PBS: 8.1 mM Na<sub>2</sub>HPO<sub>4</sub>, 1.5 mM KH<sub>2</sub>PO<sub>4</sub>, 137 mM NaCl, 2.7 mM KCl in 18 M $\Omega$  water).

Poly(dimethylsiloxane) (PDMS) microfluidic channels were fabricated according to established methods.<sup>31</sup> Briefly, a relief pattern of photoresist on a silicon wafer was created photolithographically. By curing PDMS prepolymer and cross-linker (Sylgard 184, Dow Corning; Midland, MI) 10:1 by weight against this relief structure, a negative of the relief was formed in the PDMS. The microchannels measured 200  $\mu$ m wide by 10–15  $\mu$ m deep. The device was through-bored at the ends of the channels to allow fluids access to the channels when the PDMS device was applied to a surface. Fluid flow was driven by applying vacuum to one access point on the microchannel while connecting the other access point to a reservoir of solution.

Arrays were fabricated by placing PDMS channel structures in conformal contact with gold surfaces. Solutions consisting of 0.8–1 mM of the disulfides in 1:9 H<sub>2</sub>O/MeOH were injected into

(12) Lee, Y. C.; Lee, R. T. *Acc. Chem. Res.* **1995**, *28*, 321–327.

(13) Lee, R. T.; Lee, Y. C. *Glycoconjugate J.* **2000**, *17*, 543–551.

(14) Horan, N.; Yan, L.; Isobe, H.; Whitesides, G. M.; Kahne, D. *Proc. Natl. Acad. Sci. U.S.A.* **1999**, *96*, 11782–11786.

(15) Soltyk, A. M.; MacKenzie, C. R.; Wolski, V. M.; Hiram, T.; Kitov, P. I.; Bundle, D. R.; Brunton, J. L. *J. Biol. Chem.* **2002**, *277*, 5351–5359.

(16) Kitov, P. I.; Sadowska, J. M.; Mulvey, G.; Armstrong, G. D.; Ling, H.; Pannu, N. S.; Read, R. J.; Bundle, D. R. *Nature* **2000**, *403*, 669–672.

(17) Kitova, E. N.; Kitov, P. I.; Bundle, D. R.; Klassen, J. S. *Glycobiology* **2001**, *11*, 605–611.

(18) Mulvey, G. L.; Marcato, P.; Kitov, P. I.; Sadowska, J.; Bundle, D. R.; Armstrong, G. D. *J. Infect. Dis.* **2003**, *187*, 640–649.

(19) Duverger, E.; Frison, N.; Roche, A.-C.; Monsigny, M. *Biochimie* **2003**, *85*, 167–179.

(20) Schengrund, C.-L. *Biochem. Pharmacol.* **2003**, *65*, 699–707.

(21) Kensinger, R. D.; Yowler, B. C.; Benesi, A. J.; Schengrund, C.-L. *Bioconjugate Chem.* **2004**, *15*, 349–358.

(22) Gustafson, I. *Colloids Surf. B* **2003**, *30*, 13–24.

(23) Critchley, P.; Clarkson, G. J. *Org. Biomol. Chem.* **2003**, *1*, 4148–4159.

(24) Kuziemko, G. M.; Stroh, M.; Stevens, R. C. *Biochemistry* **1996**, *35*, 6375–6384.

(25) MacKenzie, C. R.; Hiram, T.; Lee, K. K.; Altman, E.; Young, N. M. *J. Biol. Chem.* **1997**, *272*, 5533–5538.

(26) Pale-Grosdemange, C.; Simon, E. S.; Prime, K. L.; Whitesides, G. M. *J. Am. Chem. Soc.* **1991**, *113*, 12–20.

(27) Aherne, D.; Rao, S. N.; Fitzmaurice, D. *J. Phys. Chem. B* **1999**, *103*, 1821–1825.

(28) Kitov, P. I.; Railton, C.; Bundle, D. R. *Carbohydr. Res.* **1998**, *307*, 361–369.

(29) Kitov, P. I.; Paszkiewicz, E.; Wakarchuk, W. W.; Bundle, D. R. *Methods Enzymol.* **2003**, *362*, 86–105.

(30) Mulvey, G.; Vanmaele, R.; Mrazek, M.; Cahill, M.; Armstrong, G. D. *J. Microbiol. Methods* **1998**, *32*, 247–252.

(31) Xia, Y.; Whitesides, G. M. *Angew. Chem., Int. Ed. Engl.* **1998**, *37*, 550–575.

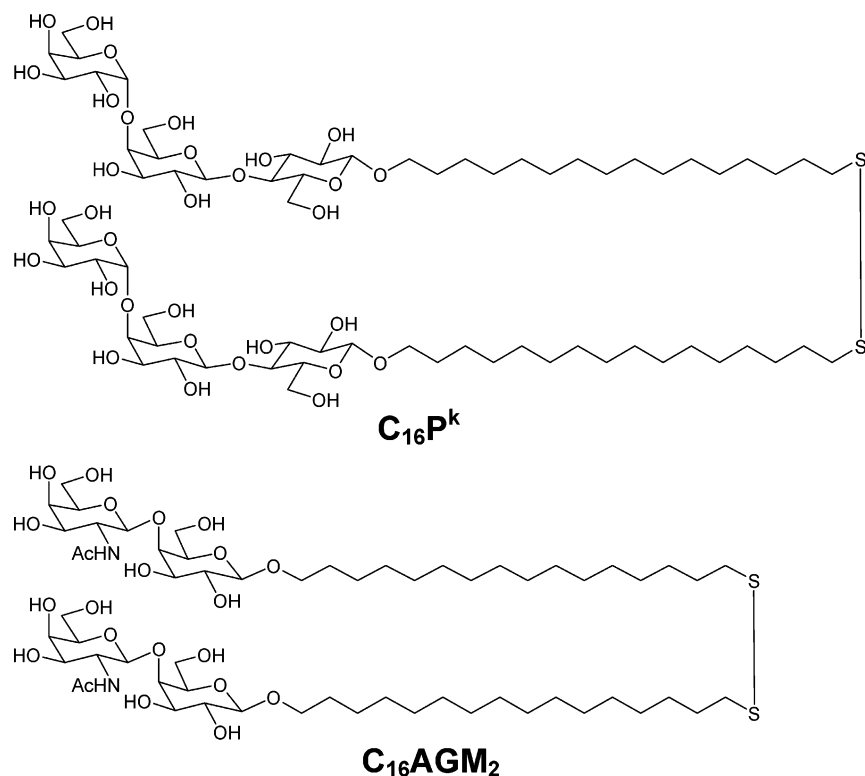


**Figure 1.** Chemical structures of C<sub>16</sub> disulfide-modified P<sup>k</sup> trisaccharide and Asialo-GM<sub>2</sub> disaccharide used to produce arrays for studies of SLT inhibition.

the channels, and the probe glycosides were allowed to adsorb for 20 min. The solvent ratio employed allowed for facile solubilization of the reagents and retained sealing of native PDMS microchannels against the gold sensor surface for the required time. Following patterning inside the channels, the entire chip was immersed into a 1 mM ethanolic solution of EG3-OME overnight.

All SPR imaging utilized sensing films consisting of 45-nm gold films deposited on SF10 glass (Schott; Toronto, ON, Canada) with a 1-nm adhesive layer of chromium. Imaging was performed using the GWC Instruments SPRImager (GWC Instruments; Madison, WI). Images displayed are averages of 100 individual snapshot images. All images were collected in toxin-free PBS. Difference images result from the subtraction of images before and after toxin binding. All accompanying image profiles are directional averages over the entire displayed image. Infrared reflection absorption spectroscopy (IRRAS) was performed on a Mattson Infinity spectrometer with an externally housed low-noise MCT-A detector at a resolution of 2 cm<sup>-1</sup>. Glycoside monolayer samples for IRRAS analysis were prepared on glass microscope slides coated with 10 nm of Cr and 300 nm of gold. Solutions consisting of total disulfide concentration of 0.9 mM were pressed between a clean glass slide and a gold slide for 20 min. This procedure was used in order to confine the small volume (50–200 μL) of glycoside solution employed.

## RESULTS AND DISCUSSION

**Array Fabrication/Optimization.** The arrays for detection of the toxin by SPR imaging were fabricated on thin gold films by patterning probe glycosides. The P<sup>k</sup> trisaccharide, which is known to bind SLT, and an asialo-GM<sub>2</sub> disaccharide, which is

expected to have no interaction with the SLT, were synthesized as hexadecanyl disulfides for easy immobilization to gold. The structures of the two disulfides are shown in Figure 1. IRRAS experiments show that immersion of gold substrates into solutions containing these disulfides results in densely packed monolayers presenting the glycoside to the interface (data not shown). Studies have shown that monolayers formed from disulfides are indistinguishable from those formed from the corresponding thiol and are likely adsorbed via thiolate–gold interactions following cleavage of the disulfide bond.<sup>32</sup> Arrays to study the binding of SLT were fabricated by patterning C<sub>16</sub>P<sup>k</sup> and C<sub>16</sub>AGM<sub>2</sub> onto SPR imaging chips using microfluidic networks in PDMS. Self-assembly of C<sub>16</sub>P<sup>k</sup> and C<sub>16</sub>AGM<sub>2</sub> to the gold substrate inside the channels resulted in ~200-μm-wide lines of glycoside-terminated monolayers. The chip was immersed in an ethanolic solution of HS(CH<sub>2</sub>)<sub>11</sub>(OCH<sub>2</sub>CH<sub>2</sub>)<sub>3</sub>OCH<sub>3</sub> (C<sub>11</sub>EG3-OME), which forms a protein-resistant background on the remaining areas of the gold. No significant displacement of the glycoside monolayers by the EG3-OME is observed by IRRAS.

SPR imaging can be used to assess the effectiveness of our procedure for fabricating arrays of glycosides. Figure 3A is the SPR image of an initial array surface featuring two lines each of C<sub>16</sub>P<sup>k</sup> and C<sub>16</sub>AGM<sub>2</sub>. The cross-sectional profile in Figure 3B reveals a pattern of intensity characteristic of glycoside monolayers formed inside the channels of the PDMS microfluidic network. The patterned glycoside regions show higher reflected intensity, implying a greater refractive index relative to the EG3-OME background. The reflectivity at the P<sup>k</sup> addresses is observably

(32) Jung, C.; Dannenberger, O.; Xu, Y.; Buck, M.; Grunze, M. *Langmuir* **1988**, *14*, 1103–1107.

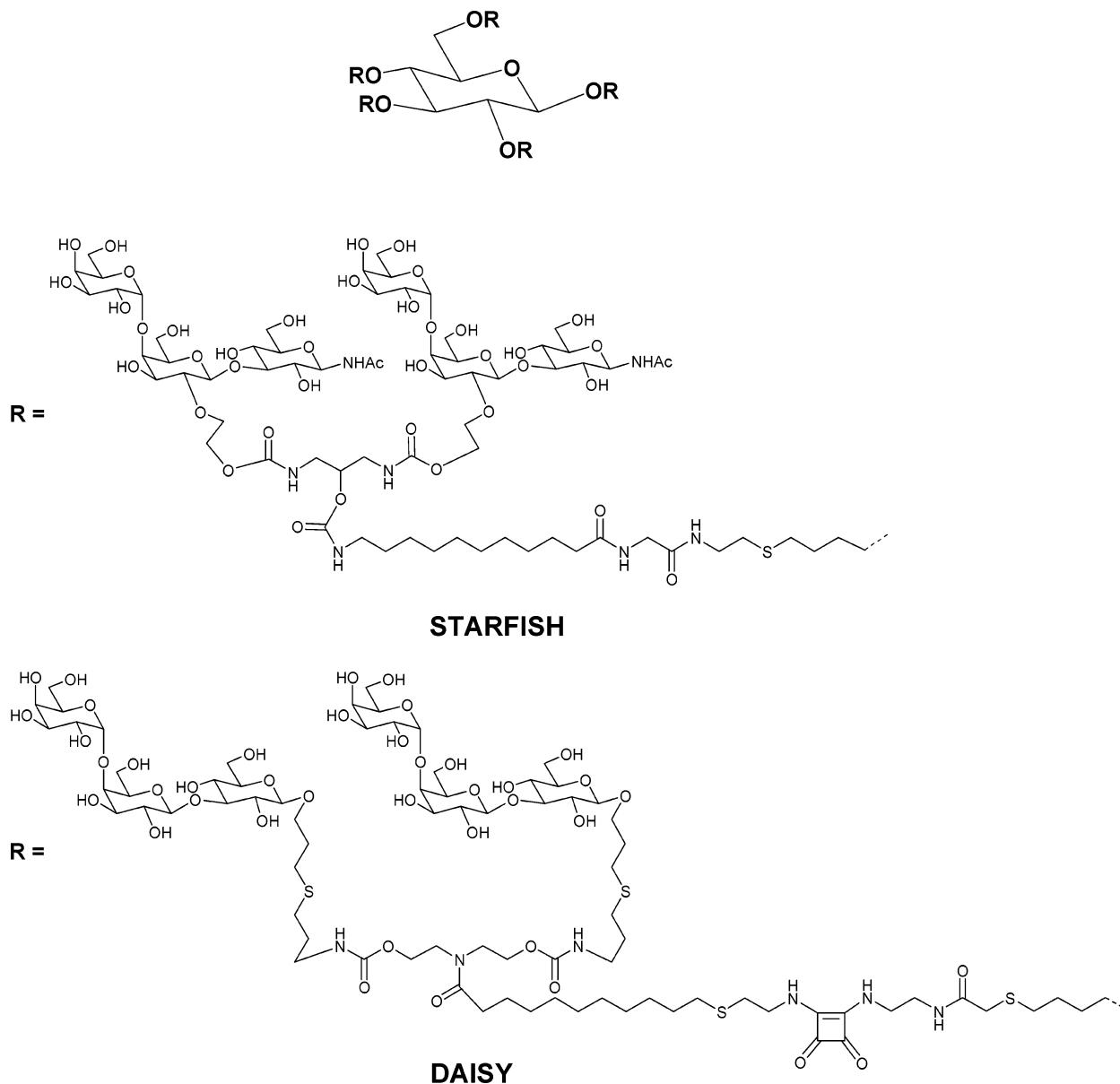


**Figure 2.** Chemical structure of starfish 2 inhibitor (FW 8703.8847) and the daisy 1 inhibitor (FW 9660.79). The P<sup>k</sup> trisaccharide unit is presented twice at each end of five radial spacer arms.

higher due to the larger mass of the C<sub>16</sub>P<sup>k</sup> inducing a greater change in refractive index.

The differential binding of SLT by the C<sub>16</sub>P<sup>k</sup>/C<sub>16</sub>AGM<sub>2</sub> array is demonstrated by SPR imaging as shown in Figure 3C and D. Figure 3C is the difference image following the exposure of the array to 130 nM SLT for 10 min and rinsing with PBS. The cross-sectional profile in Figure 3D reveals an increase in signal on the P<sup>k</sup> trisaccharide addresses, with no detectable adsorption on either the C<sub>16</sub>AGM<sub>2</sub> or the EG3-OME background. The magnitude of the signal change observed in Figure 3D for SLT binding (15 RU) is similar to that observed for the C<sub>16</sub>P<sup>k</sup> addresses (11 RU) on the original chip, Figure 3B. Based on previous observed signal changes for IgG antibodies (MW = ~150 000) of 50–60 RU,<sup>33</sup> a signal of 15 RU for the binding of the ~40 000 SLT is reasonable. Thus, the differences in reflectivity observed on the original

glycoside chip (Figure 3B) are too large to be ascribed only to mass differences. Although speculative at this time, the interaction of the buffer solution with the various surface moieties may contribute to the contrast of the glycoside chip. Despite this uncertainty, the signals shown in Figure 3C indicate selective binding and demonstrate that patterned monolayers of C<sub>16</sub>P<sup>k</sup> show specific affinity for SLT that is detectable by SPR imaging.

Given the fixed locations of the binding sites on the SLT B<sub>5</sub> subunit, the effect of the surface density of C<sub>16</sub>P<sup>k</sup> was studied. This was accomplished by measuring the amount of SLT binding to mixed monolayers of C<sub>16</sub>P<sup>k</sup> and a diluent species. Considering the insignificant amount of SLT bound to C<sub>16</sub>AGM<sub>2</sub> shown in Figure 3D, we conclude that monolayers composed of interfacial oligosaccharide groups are quite resistant to nonspecific protein adsorption. While monolayers presenting mannitol groups at the surface have been shown to be at least as protein-resistant as oligo-(ethylene glycols),<sup>34</sup> the observation has not been generalized to

(33) Kanda, V.; Kariuki, J.; Harrison, D. J.; McDermott, M. T. *Anal. Chem.* **2004**, *76*, 7257–7262.

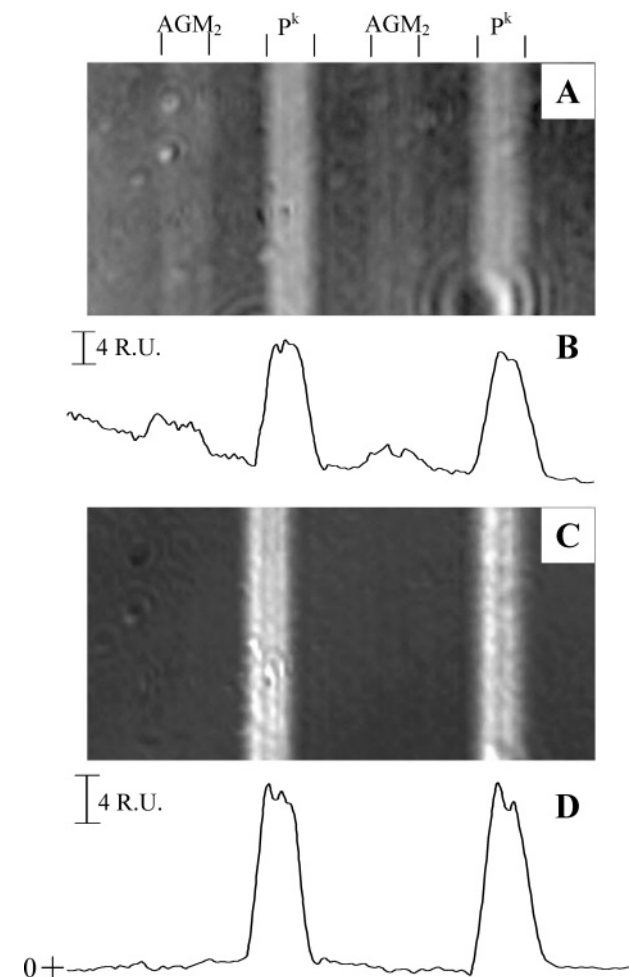


**Figure 3.** (A) SPR image of the initial  $C_{16}AGM_2$  and  $C_{16}P^k$  array. (B) Cross section showing greater initial signal on the  $P^k$  regions than on the  $AGM_2$ . (C) Difference image after exposure of array to 130 nM SLT for 10 min. (D) Cross section of difference image shows exclusive binding to  $P^k$ ; cross indicates the zero signal level for the difference image.

a broader class of saccharide-terminated films. The property of protein resistance would come as little surprise given the role of cell surface saccharides in specific protein recognition. Given this resistance to SLT nonspecific adsorption, the  $AGM_2$  species was used as a diluent for varying the surface density of the  $P^k$  trisaccharide.

The effect of diluting  $C_{16}P^k$  with  $C_{16}AGM_2$  on SLT binding is shown in Figure 4. Four lines were arrayed from solutions containing varying mole fractions ( $\chi$ ) of  $C_{16}P^k$  relative to  $C_{16}AGM_2$ . A number of studies have shown that the surface density of one component of a two-component monolayer can be controlled by varying the ratio in solution.<sup>35–37</sup> Note that the IR spectral differences between  $C_{16}P^k$  and  $C_{16}AGM_2$  are minimal and are insufficient to directly determine the surface density of each glycoside. We thus describe the array addresses of mixed glycoside monolayers by the mole fraction of  $C_{16}P^k$  in the assembly

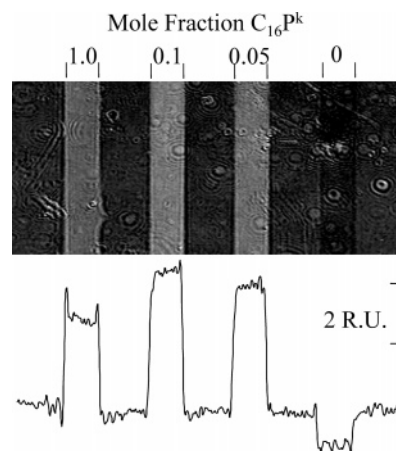


**Figure 4.** SPR difference image and cross-sectional profile following exposure of a glycoside array to 130 nM SLT for 10 min. The array elements were prepared from solutions containing both  $C_{16}P^k$  and  $C_{16}AGM_2$  (total concentration, 0.9 mM). Each element is labeled with the mole fraction of  $C_{16}P^k$  used in the assembly solution.

solution. Figure 4 contains the difference image following exposure of the array to SLT. The cross-sectional profile shows negligible SLT binding on the  $C_{16}AGM_2$  line ( $\chi = 0$ ) and a small amount of nonspecific adsorption to the  $C_{11}EG3-OMe$  background on this chip. The profile also reveals maximal SLT binding at this array does not occur at single-component monolayers of  $C_{16}P^k$  but at addresses prepared from solutions of  $\chi = 0.1$ . This implies that the surface density of glycoside receptors is important to optimal toxin binding. This observation is explored in more detail with IRRAS.

The absorbance of the amide II band is thought to correlate linearly with the amount of adsorbed protein,<sup>38,39</sup> making it a good diagnostic band for SLT adsorption. By tracking the changes in the amide II band intensity upon SLT binding to mixed  $C_{16}P^k/C_{16}AGM_2$  monolayers, it was possible to determine the optimal  $C_{16}P^k$  solution  $\chi$ . Figure 5A shows infrared spectra of a monolayer prepared from a 0.1 mol fraction solution of  $C_{16}P^k$  before and after adsorption of SLT. Measurements of amide II band intensity were made after subtracting the spectra before and after SLT adsorption, thus normalizing for variations in the spectra of the initial glycoside monolayers.

The plot in Figure 5B shows the change in amide II intensity for SLT binding with  $C_{16}P^k$  mole fraction in solution. This plot shows very little SLT binding at low  $\chi$  of  $C_{16}P^k$ , a maximum in binding at  $\chi \sim 0.15$ , and a slight decrease as the solution concentration is increased. This observation points to an optimal surface density of  $C_{16}P^k$  for SLT binding that is less than 100%. A previous SPR imaging study showed that the binding of lectins reaches a limiting value when the surface density of immobilized monosaccharide epitopes is below 100%.<sup>6</sup> Our results are not surprising given that SLT contains a series of spatially well-defined binding sites and achieves maximum binding strength through 5-fold multivalent interactions with  $Gb_3$  glycolipids. Figure 5B suggests that monolayers formed from solutions containing 10–15%  $C_{16}P^k$  provide the optimum interfacial distribution of the  $P^k$

(34) Luk, Y.-Y.; Kato, M.; Mrksich, M. *Langmuir* **2000**, *16*, 9604–9608.

(35) Chidsey, C. E. D.; Bertozzi, C. R.; Putvinski, T. M.; Mujisce, A. M. *J. Am. Chem. Soc.* **1990**, *112*, 4301–4306.

(36) Folkers, J. P.; Laibinis, P. E.; Whitesides, G. M.; Deutch, J. J. *Phys. Chem.* **1994**, *98*, 563–571.

(37) Kwon, Y.; Mrksich, M. *J. Am. Chem. Soc.* **2002**, *124*, 806.

(38) Jakobsen, R. J.; Brown, L. L.; Winters, S.; Gendreau, R. M. *J. Biomed. Mater. Res.* **1983**, *16*, 199–201.

(39) Liedberg, B.; Ivarsson, B.; Lundstrom, I. *J. Biochem. Biophys. Methods* **1984**, *9*, 233–243.

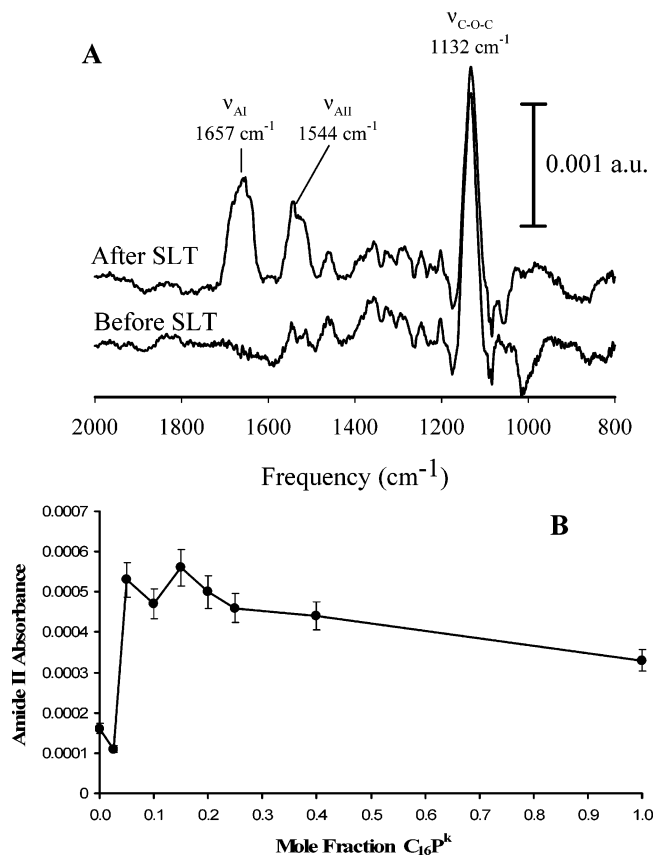


**Figure 5.** (A) IRRAS spectra of a glycoside monolayer formed from a solution containing  $\chi = 0.1$   $C_{16}P^k$  before and after incubation in 130 nM SLT. (B) Amide II band ( $\nu_{AII}$ ) intensity vs mole fraction  $C_{16}P^k$  for SLT binding to a range of mixed glycoside monolayers. The error bars correspond to the standard deviation of two to three measurements.

trisaccharide to enable multivalent interactions with SLT. We attribute the slight decrease in observed SLT binding at higher  $\chi$  to crowding of surface-bound  $P^k$  that may lead to inhibitory intermolecular interactions or steric effects.

**Inhibition Studies.** Having determined an optimal surface density of  $C_{16}P^k$  for SLT binding, assays were performed to study the inhibitory effect of synthetic pentameric ligands. Figure 2 shows the SF-2 and Daisy ligands used to bind the toxin. Each structure was designed in such a way that the terminal carbohydrate fragments would be able to occupy the strong binding sites of the toxin (there are 10 additional weak binding sites). The inhibition of SLT activity by multivalent starfish and daisy ligands has been previously demonstrated by ELISA<sup>16,18</sup> and mass spectrometry<sup>17</sup> as well as by *in vitro*<sup>16</sup> and *in vivo*<sup>18</sup> studies. The principal ELISA methods used required separate steps for labeling, blocking, binding interaction, and color development for detection. The inhibition of SLT was studied in order to demonstrate the efficacy and simplicity of microfluidic patterning and SPR imaging as an alternative to ELISA.

Assays were performed by exposing  $C_{16}P^k$  arrays to 1.6  $\mu\text{g}/\text{mL}$  (42 nM) SLT in PBS with varying inhibitor concentrations and then using SPR imaging to detect the bound SLT. The key parameter in inhibition studies is  $IC_{50}$ , which is defined as the inhibitor concentration at which 50% of the toxin is inhibited. In our case,  $IC_{50}$  is the concentration of inhibitor that yields 50% of

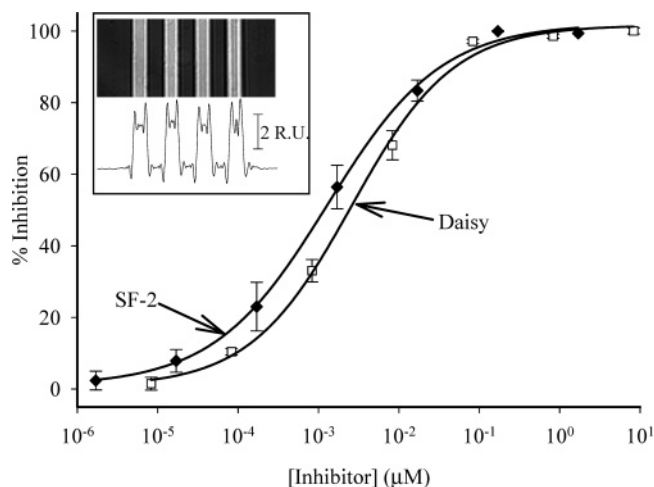


**Figure 6.** Inhibition curves for the SF-2 and daisy inhibitors. See text for details. The inset is a typical SPR image and profile showing the signal observed at the array for 42 nM SLT solutions.

the maximal SLT binding to the array surface and is analogous to previous ELISA results.<sup>16</sup> Given that SLT operates by binding to  $Gb_3$  receptors on cell walls, we believe this definition is appropriate. The curves generated from the assays were fit with eq 1, which is analogous to a four-parameter logistic model,<sup>40</sup>

$$\Delta\%R = \Delta\%R_{\min} + \frac{\Delta\%R_{\max} - \Delta\%R_{\min}}{1 + ([A]/IC_{50})^b} \quad (1)$$

where  $\Delta\%R_{\max}$  and  $\Delta\%R_{\min}$  are asymptotic signal values determined from the regression analysis,  $[A]$  is the adsorbate solution concentration, and  $IC_{50}$  is the concentration at which the inhibition is half-maximal.  $\Delta\%R_{\max}$ ,  $\Delta\%R_{\min}$ ,  $IC_{50}$ , and  $b$  are the fitting parameters. When the data are plotted on a log scale in  $[A]$ , the parameter  $b$  reflects the slope of the curve at the inflection point. When  $b = 1$ , the equation reduces to the Langmuir isotherm. Although proposed interpretations for deviations from  $b = 1$  are that  $b < 1$  implies inhomogeneity in binding affinities or negative cooperativity while  $b > 1$  indicates a positive cooperativity effect,<sup>40</sup> any real physical basis for the observed values is somewhat speculative.<sup>41</sup> The iterative least-squares solution of this equation, also known as the Hill or Sips plot, is widely used to analyze binding curves in the life sciences.<sup>42</sup>

Inhibition curves for SF-2 and daisy are shown in Figure 6 and the parameters obtained from the fits are listed in Table 1. Note that, in Figure 6, the y-axis was converted from  $\Delta\%R$  to % inhibition where,

$$\% \text{ inhibition} = 100\% - \left( \frac{\Delta\%R}{\Delta\%R_{\max} - \Delta\%R_{\min}} \right) \quad (2)$$

$\Delta\%R_{\max}$  and  $\Delta\%R_{\min}$  were obtained from the fits of  $\Delta\%R$  versus

(40) Rodbard, D.; Hutt, D. M. In *Radioimmunoassay and Related Procedures in Medicine*; IAEA: Vienna, 1974; Vol. 1, pp 165–192.

(41) Henderson, P. J. F. In *Enzyme Assays: A Practical Approach*; Eisenthal, R., Danson, M. J., Eds.; Oxford University Press: New York, 1993; pp 277–316.

(42) Nix, B.; Wild, D. In *The Immunoassay Handbook*; Wild, D., Ed.; Nature Publishing: New York, 2001; pp 198–210.

**Table 1. Curve Fitting Parameters for SF-2 and Daisy Inhibition Curves in Figure 6<sup>a</sup>**

inhibitor	IC <sub>50</sub> ( $\mu$ M)	$\Delta\%R_{\min}$	$\Delta\%R_{\max}$	b	R <sup>2</sup>
SF-2	$1.3(0.2) \times 10^{-3}$	$\sim 0$	5.6(0.1)	0.62(0.05)	0.991
daisy	$2.6(0.3) \times 10^{-3}$	$\sim 0$	5.1(0.1)	0.69(0.04)	0.996

<sup>a</sup> Values in parentheses are standard deviations of the indicated values.

log[inhibitor] plots and are given in Table 1. The inhibition values plotted reflect the fraction of the maximum signal that was *not* observed as a result of inhibitor binding to SLT.

The IC<sub>50</sub> values obtained (Table 1) are in the low-nanomolar range for each inhibitor, in agreement with ELISA work performed previously. The value of 2.6 nM for Daisy is slightly less than the reported value of 8.05 nM using ELISA (protocol B, see below).<sup>18</sup> The value of 1.3 nM for SF-2 is slightly larger than the values of 0.24 (protocol A) and 0.4 nM (protocol B) for a similar inhibitor.<sup>16</sup> The similarity in the IC<sub>50</sub> values reported here and those determined by various methods in the literature<sup>16,18</sup> imply that SPR imaging is a viable approach for inhibition studies. The clear advantages of SPR for this type of assay are operational simplicity and, more importantly, a minimization of the number of interactions necessary to produce a signal as discussed below.

In previous ELISA studies of SLT inhibition, two separate protocols, termed protocols A and B, were used and are illustrated in Figure 7.<sup>16</sup> In protocol A, SLT was coated on a 96-well ELISA plate, blocked with milk protein (MP), and then exposed to solutions with 10  $\mu$ g/mL of a biotinylated BSA-P<sup>k</sup> trisaccharide conjugate and varying concentrations of inhibitor. Analysis was performed by adding a streptavidin–horseradish peroxidase (HRP) conjugate and developing with tetramethylbenzidine (TMB)/hydrogen peroxide and phosphoric acid. The absorbance was then detected at 450 nm. In protocol B, C<sub>16</sub>P<sup>k</sup> was applied to a 96-well ELISA plate before blocking with BSA. SLT with varying inhibitor concentrations was then added. Surface-bound SLT was detected by first adding a rabbit anti-SLT antibody to bind the SLT and then adding HRP-conjugated anti-rabbit IgG antibody. The detection was again performed by developing with TMB/peroxide and reading the absorbance. A schematic comparison of the interactions employed in the ELISA protocols and the SPR imaging protocol used in this work is shown in Figure 7. The SPR imaging method is shown to be advantageous in that far fewer reaction steps are necessary in order to perform the assay. As a result, there are fewer steps at which a systematic or random error can be introduced to the assay. In addition to the time savings, by which a 2-day procedure essentially becomes a 1-day procedure, the elimination of many tedious pipetting and washing steps, which

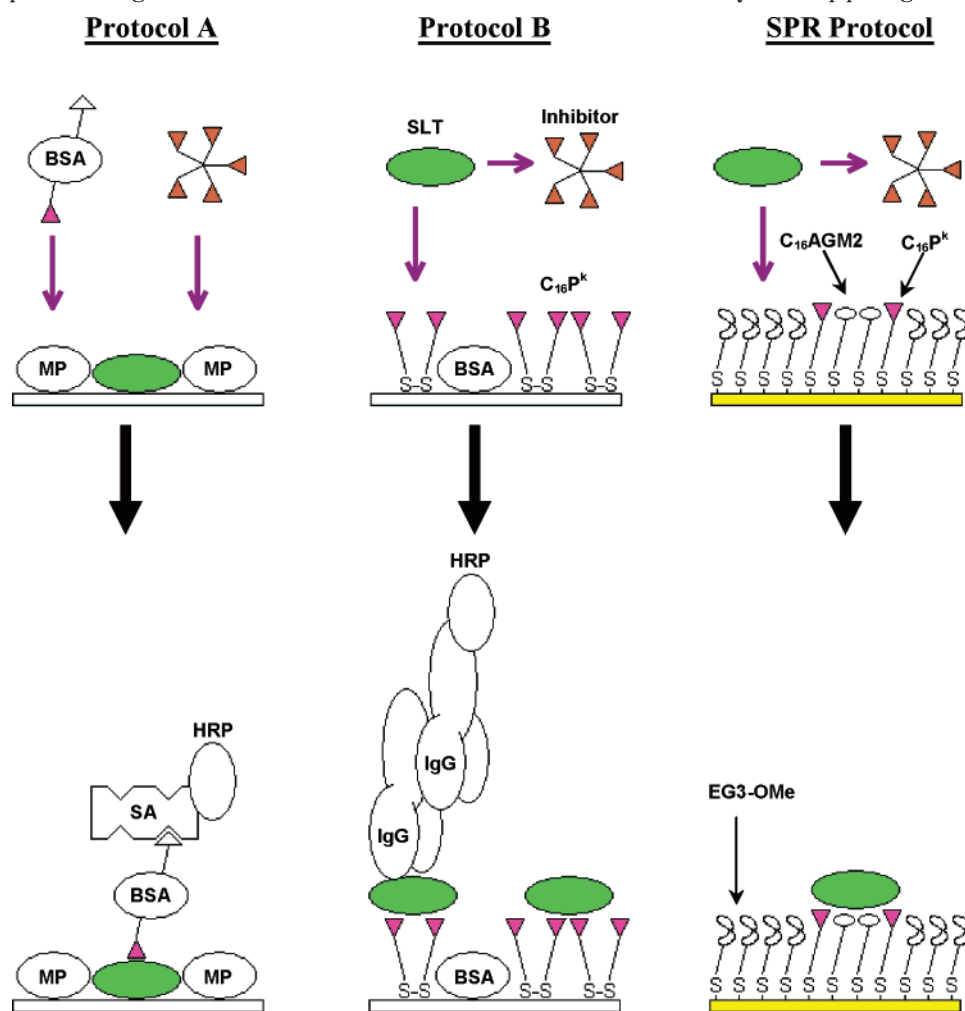


**Figure 7.** Comparison of inhibition assay procedures. Protocol A and protocol B are ELISA-based assays used in previous work.<sup>16</sup> The SPR protocol is used in this work. The top row illustrates the assay format while the bottom row illustrates the detection method. See text for assay details. BSA, bovine serum albumin; MP, milk protein; SA, streptavidin; HRP, horseradish peroxidase.

require high precision and training, is a major advantage of the SPR imaging methodology presented. The color development step for detection is a kinetic process that also requires a high degree of precision.

## CONCLUSIONS

More efficient assays will emerge with the development of facile and reliable methods to pattern biomolecules on to surfaces and with new, sensitive, label-free detection schemes. We have demonstrated that SPR imaging is a viable technique for label-free screening of toxin inhibition. Patterning of disulfide glycosides on gold with PDMS microfluidic networks provides an easy and effective means of fabricating carbohydrate arrays for SPR imaging. In this work, SLT binding was maximized by lowering the surface receptor density to a level reflecting 15% mol fraction in solution. The inhibition assays demonstrated here provided similar  $IC_{50}$  values to ELISA protocols but were shown to be far simpler and reliant upon fewer interactions. Although a low density of

array elements was explored here, this methodology can be scaled to fabricate a higher density of addresses (10–100) for screening glycoside libraries.

## ACKNOWLEDGMENT

This work was supported by the Natural Sciences and Engineering Research Council of Canada (NSERC). We thank the U of A NanoFab for the use of their facility in the fabrication of masters and PDMS microfluidic networks and the U of A for support of the Nanofab.

## SUPPORTING INFORMATION AVAILABLE

Additional information as noted in text. This material is available free of charge via the Internet at <http://pubs.acs.org>.

Received for review March 10, 2005. Accepted August 18, 2005.

AC050423P